Research Article

Subramani Naveen Kumar*, Visvalingam Balasubramanian, Sudersanan Malarvizhi, Abdur Hafeezur Rahman, and Vadivel Balaguru

Effect of welding consumables on shielded metal arc welded ultra high hard armour steel joints

https://doi.org/10.1515/jmbm-2022-0002
Received May 21, 2021; accepted Sep 23, 2021

Abstract: Materials with high hardness are usually preferred in armour applications and are difficult to weld due to high Carbon Equivalent (C.E). In this investigation, an attempt was made to weld Ultra-high Hard Armour (UHA) steel (having C.E of 0.91) by Shielded Metal Arc Welding (SMAW) process using three electrodes (i) austenitic stainless steel (ASS- E307-16), (ii) super duplex stainless steel (SDSS-E2594-16) (iii) low hydrogen ferritic (LHF-E12018M-low-alloy steel electrode). The mechanical properties (tensile, impact toughness, and microhardness) were evaluated and correlated with microstructural features along with Cr_{eq}/Ni_{eq} ratio of weld metal. The joints fabricated using LHF electrodes showed superior strength of 962 MPa and hardness of 341 HV. The joints made using ASS electrode showed superior impact toughness of 72 J and Notch Strength Ratio (NSR) of 1.32 due to the higher energy absorption capability of the austenitic phase. At the weld interface, joints fabricated using ASS and SDSS electrodes show the unmixed zone (UMZ) and martensitic band (MB) due to sudden change of crystal structure (Face Centred Cubic (FCC) / Body Centred Tetragonal (BCT)). It is also found that the strength property increases (651 MPa to 856 MPa) with an increase in Cr_{eq}/Ni_{eq} ratio (1.87 to 3.2) of weld metal and with a decrease in ductility.

Keywords: Ultra-high hard armour steel, shielded metal arc welding, tensile properties, impact toughness, microhardness, microstructure

Abbreviations

UHA	Ultra high Hard Armour
SMAW	Shielded Metal Arc Welding
C.E	Carbon Equivalent
ASS	Austenitic Stainless Steel
SDSS	Super Duplex Stainless Steel
LHF	Low Hydrogen Ferritic
UMZ	Unmixed Zone
MB	Martensitic Band
FCC	Face Centered Cubic
BCT	Body Centered Tetragonal
AFVs	Armour Fighting Vehicles
MBTs	Main Battle Tanks
RHA	Rolled Homogenous Armour
GMAW	Gas Metal Arc Welding
K-TIG	Keyhole Tungsten Inert Gas
HIC	Hydrogen-Induced Cracking
HAZ	Heat-Affected Zone
EDM	Electric Discharge Machining
WPS	Welding Procedure Specification
WPQR	Welding Procedure Qualification Record
ASME	American society of mechanical engineers
SUUA	Joints made by SMAW process using ASS electrodes
SUUD	Joints made by SMAW process using SDSS electrodes
SUUF	Joints made by SMAW process using LHF electrodes
VT	Visual Inspection
PAUT	Phased Array Ultrasonic Testing Machine
ASTM	American Society for Testing & Materials
NSR	Notch Strength Ratio
SEM	Scanning Electron Microscopy
BM	Base Metal
FGHAZ	Fine Grain Heat Affected Zone
CGHAZ	Coarse Grain Heat Affected Zone
ICHAZ	Inter-Critical Heat Affected Zone
OES	Optical Emission Spectrometer

***Corresponding Author: Subramani Naveen Kumar:** Centre for Materials Joining and Research (CEMAJOR), Department of Manufacturing Engineering, Annamalai University, India; Email: kumbikesavan@gmail.com
Visvalingam Balasubramanian, Sudersanan Malarvizhi: Centre for Materials Joining and Research (CEMAJOR), Department of Manufacturing Engineering, Annamalai University, India
Abdur Hafeezur Rahman, Vadivel Balaguru: Main Battle Tank Division (MBT), Combat Vehicles Research & Development Establishment (CVRDE), DRDO, Avadi, Chennai India

1 Introduction

The weight reduction in armour fighting vehicles (AFVs) is attained through materials engineering and design optimization. Weight reduction by materials engineering delivers structural efficiencies (improve mobility in the high terrain region), reduces material usage, and benefits cost reduction. Currently, rolled homogenous armour (RHA) used in the Main Battle Tanks (MBTs) [1] have crossed a total weight of 60 tonnes, which reduces mobility and transportability. Hence, designers have developed ultra-high hard armour (UHA) steel with 600 BHN hardness and 2100 MPa ultimate tensile strength, which is twice the hardness and strength of RHA steels. UHA steels attain their strength and toughness through control over chemical composition and heat treatment. Due to the high hardness of these steels, the welding processes and welding consumables decide the microstructure of the weldment. These steels are welded using commonly known processes such as Gas Metal Arc Welding (GMAW) and Shielded Metal Arc Welding (SMAW) to attain high quality and cost-effective methods for the fabrication of AFVs [2].

Some studies were carried out using Keyhole-Tungsten Inert Gas (K-TIG) welding to weld 9 mm thick plates in a single pass (welded without edge preparation). The bainite in the weld metal improved the weld joint efficiency than the conventional welding processes and consumables [3]. Hybrid welding (Laser and TIG) was used to weld 15 mm thick armour steel in two passes. The joints showed 1.6 times higher strength than the base metal by altering the mechanical properties and chemical composition [5, 6]. Weld thermal cycle (heating and cooling) during welding promotes significant changes in weld metal microstructure [7]. These steels are affected by Hydrogen-Induced Cracking (HIC) and Heat-Affected Zone (HAZ) softening issues [8]. The problem with the SMAW is process is the use of coated electrodes. Selection of electrode and its coating is important to be consider to avoid cold cracking. Some studies are carried to understand the effects of different hydrophobic coatings on the surface of covered basic electrodes on the quality of wet welded carbon steel joints. The waterproof coatings laid on covered electrodes decreasing the Vickers hardness by 10 HV in heat-affected zone (HAZ) and decreasing the diffusible hydrogen content in deposited metal, which minimalize possibility of cold cracking [9]. In another study rutile-based electrode were used to study the effect of storage time of electrode in cold cracking. Results shows that storage time of the electrodes does not have a significant influence on the content of diffused hydrogen in the deposited metal [10]. Presence of high hydrogen content in the weldment can change the mode of failure from ductile + brittle to complete brittle failure [11].

ASS consumables are one solution to control the HIC problem due to the higher solubility of hydrogen in the austenite phase [12]. Another important factor for considering ASS consumable is the reduction of thermal stresses, migration of carbon towards weld metal [13], and to obtain impact toughness 15 J at −40°C (min requirement) in welding of armour steels.

The matching high strength electrodes can't satisfy the above-said problems, and more over-development of such electrodes which match the base metal properties are still under development. An alternative way to improve the structural properties (mechanical properties) by addressing those issues to some extent is modifying the Cr_{eq}/Ni_{eq} ratio [14]. SDSS electrodes are one such solution by improved Cr_{eq}/Ni_{eq} ratio, which can produce an equal amount of ferrite and austenite and improves the strength properties. Use of an alternative low-cost consumable, LHF, an alternative to ASS electrode in the welding of armour steel, and high tensile strength with no occurrence of HIC is possible [15]. Proper selection of electrodes for welding of armour steels reduces welding problems and improves mechanical properties [16, 17]. Solidification cracking in the weld metal is controlled by a minimum of 3% delta ferrite in the weld metal [18]. The small amount of delta ferrite determines the service requirements [19, 20]. Ni based electrodes are not cost effective along with they need to justify the other important properties such as ballistic performance. These electrodes (ASS, SDSS, LHF) are already ballistic proven electrodes (Stopped the Armour piercing (AP) projectile). Softening can be controlled effectively using a low heat input process, reducing the HAZ width [21].

From the above literature, it is understood that welding consumables have a significant effect on the performance of the joints. Research works focussed on welding of armour steels are very few in numbers, especially on UHA steels. To eliminate the research gap on welding of high hardness, armour steels, and the data on the fabrication of joints in the real-time application (MBTs and AFVs) are needed. Hence, in this investigation, the effect of welding consumables on mechanical properties of shielded metal arc welded ultra-high hard armour steel joints is investigated and the results are discussed in details.

2 Experimental work

The base metal (BM) used in this investigation was 15 mm thick high strength, low alloy ultra-high hard armour

Table 1: Chemical composition (wt %) of base metal and electrodes (deposited metal)

Material	C	Si	Mn	P	S	Cr	Mo	Ni	Fe
BM	0.346	0.240	0.56	0.007	0.007	1.26	0.54	1.27	Bal
ASS	0.076	0.43	1.24	0.022	0.008	18.31	2.41	9.23	Bal
SDSS	0.026	0.72	1.76	0.018	0.006	24.3	3.45	7.12	Bal
LHF	0.041	0.342	1.42	0.025	0.004	0.153	0.215	2.41	Bal

Table 2: Mechanical properties of base metal and electrodes (deposited metal)

Material	0.2% Yield strength (MPa)	Ultimate tensile strength (MPa)	Elongation in 50 mm gauge length (%)	Impact toughness at RT (J)	Hardness at 0.5 kg load (HV)
BM	1451	2151	11	42	602
ASS	633	702	23	66	225
SDSS	764	873	21	55	286
LHF	838	975	18	48	312

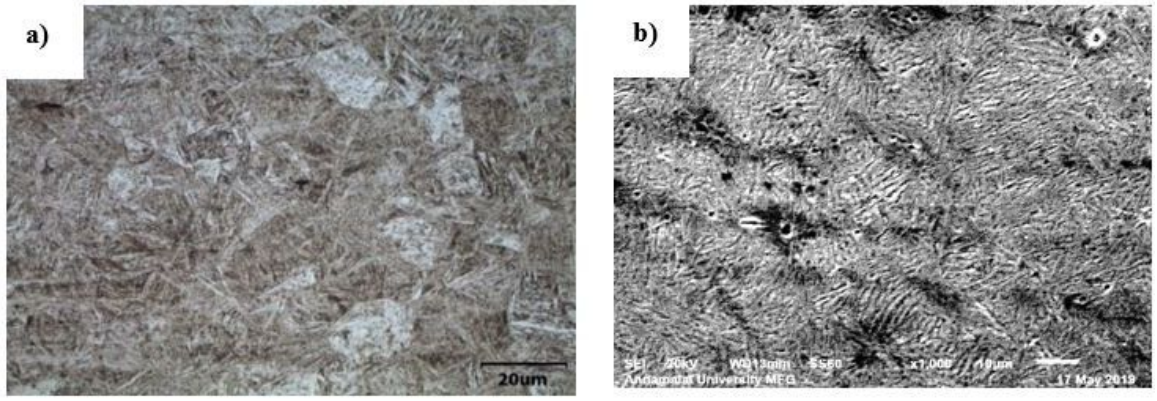

Figure 1: Micrograph of base metal; (a) Optical microscopy image of BM; (b) Scanning electron microscopy image of BM

steel (UHA) (Armox 600T closely conform to AISI 4340) in quenched and tempered condition (Q&T). The base metal chemical composition and mechanical properties are listed in Tables 1 and 2, respectively. The base metal microstructure consists of tempered martensite in the ferrite matrix (shown in Figure 1). Rolled plates were machined to 300 × 150 mm by cutting, and a single 'V' groove butt joint was made using wire cut electric discharge machining (EDM) process, as shown in Figure 2a. The joints were fabricated using the shielded metal arc welding (SMAW) machine (Make:Lincoln Electric (USA)). The welding parameters and welding conditions used to fabricate the joints are presented in Table 3. Welding procedure specification (WPS) and welding procedure qualification record (WPQR) established for these steels in our centre according to sec IX ASME (American society of mechanical engineers) were used as welding parameters. In total, seven passes were deposited to fabricate the joints using the SMAW process. No welding pads are used. The electrode used in this investigation are:

(i) Basic coated austenitic stainless steel (ASS) consumable closely conforms to AWS E307
(ii) Basic coated super duplex stainless steel (SDSS) closely conforms to AWS E2594
(iii) Basic coated low hydrogen ferritic (LHF) closely conforms to AWS E12018M

To understand better, joints fabricated are referred as

(i) SUUA (joints made by SMAW process using ASS electrodes)
(ii) SUUD (joints made by SMAW process using SDSS electrodes)
(iii) SUUF (joints made by SMAW process using LHF electrodes)

Table 3: Welding parameters used for fabrication of joints

Parameter	Unit	SUUA Joint	SUUD Joint	SUUF Joint
Electrode specification	AWS	**SFA 5.4, E307-16**	**SFA5.4, E2594-16**	**SFA 5.5, E12018M**
Electrode drying temperature	°C	150 for 1hr	150 for 1hr	200 for 3hr
Current and Polarity		DCEP	DCEP	DCEP
Welding position (EN ISO 6947)		PA flat-1G	PA flat-1G	PA flat-1G
Preheat temperature	°C	150	150	150
Interpass temperature	°C	200	200	200
Thermal efficiency (K)			0.80	
		For Filling Pass		
Electrode diameter	mm	4.00	4.00	4.00
Welding current	A	140	160	150
Arc voltage	V	28	28	27
Welding speed	mm/min	205	195	210
Average heat input/pass	kJ mm^{-1}	**1.14**	**1.37**	**1.15**

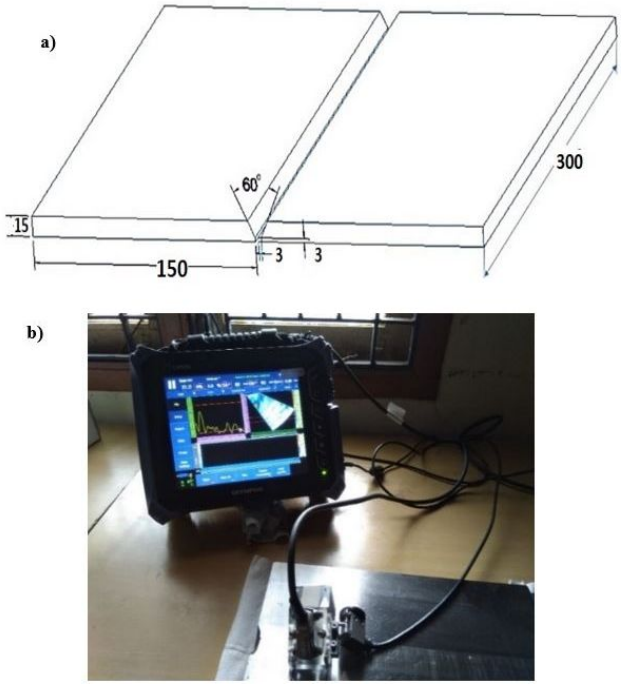

Figure 2: Welding details; (a) Joint configuration; (b) PAUT scanner used for the soundness of weld

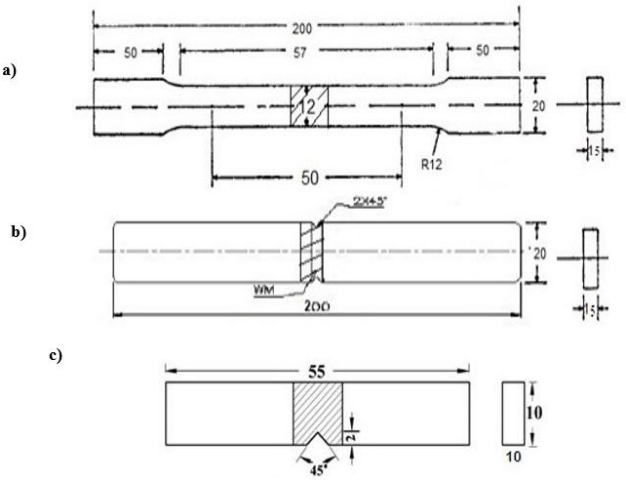

Figure 3: Dimensions of the specimens a) Smooth tensile specimen, b) Notch tensile specimen c) Impact toughness specimen

The soundness of the joints was tested using visual inspection (VT) and phased array ultrasonic testing machine (PAUT) scanner (Make: OLYMPUS, USA Model: HST-LITE-KIT01). Visual examination of weld joint is an important activity, carried out to check the integrity of the weldment. Visual inspection is carried out before and after welding in illumination of 500 Lux with the inspector eye of within the radii of 600 mm of the surface and viewing angle of greater than 30 degrees.

Before welding the base metal and electrodes are inspected along with joint preparation and alignment are checked with weld gap gauge, vernier calibre and magnifying glass. After welding using welding gauge complete visual inspection is done on surface defects and PAUT scanner was used to find the internal defects as shown in Figure 2b. American Society for Testing & Materials (ASTM), guidelines were used to evaluate the tensile and impact toughness properties of base metal and welded joints. The smooth (unnotched) tensile specimens were prepared (Figure 3a) to evaluate the yield strength, tensile strength, and

elongation. To evaluate the joint's notch tensile strength and notch strength ratio (NSR), notch tensile specimen were used as shown in Figure 3b. The tensile test was carried out in a 1000 kN, electro-mechanical controlled universal testing machine (Make:FIE-BLUESTAR, Capacity:1000 kN). The specimen was loaded at the rate of 1.5 kN min^{-1} as per specification (ASTM E8M-04) so that the tensile specimen undergoes uniform deformation. The specimen finally fails after necking, and the load versus displacement was recorded. The 0.2% offset yield strength was derived from the diagram.

The Charpy impact test was conducted at room temperature using a pendulum-type impact testing machine. A Vickers microhardness testing machine was employed for measuring the hardness across and along the weld. Hardness was measured at the distance of 0.5 mm with a 500 g load for all joints. Optical emission spectroscopy (OES) was used to determine the chemical composition of the diluted weld metal. X-ray diffraction (XRD) was used to analysis the phases present in the weld metal of the joints.

The microstructure analysis of the weldments was carried out using a light optical microscope. The specimens were etched with a 2% Nital reagent to reveal the microstructure of the weld region of the LHF joint, BM, and HAZ regions. Aqua regia and Kalling's reagent were used to reveal the microstructure of the ASS weld and SDSS weld regions, respectively. The tensile and impact specimen's fractured surface was analyzed using a scanning electron microscopy (SEM) to study the nature of the fracture.

3 Results

3.1 Tensile properties

The tensile properties of base metal and deposited metal are shown in Table 2. In comparison, the transverse tensile properties of welded joints are shown in Table 4. Three specimens were tested in each condition, and the average of three results is presented and Figure 4 shows the stress-strain curves recorded during tensile test.

From the above results, (i) All the tensile specimen failed at weld metal (WM) region only, irrespective of welding consumables; (ii) The SUUF joints exhibited the highest tensile strength of 962 MPa, 47% of base metal strength; (iii) The SUUA joints exhibited the highest elongation (ductility) of 24% (iv) The SUUA joints showed the highest NSR (ductility parameter) of 1.32. (v) In comparison, SUUA

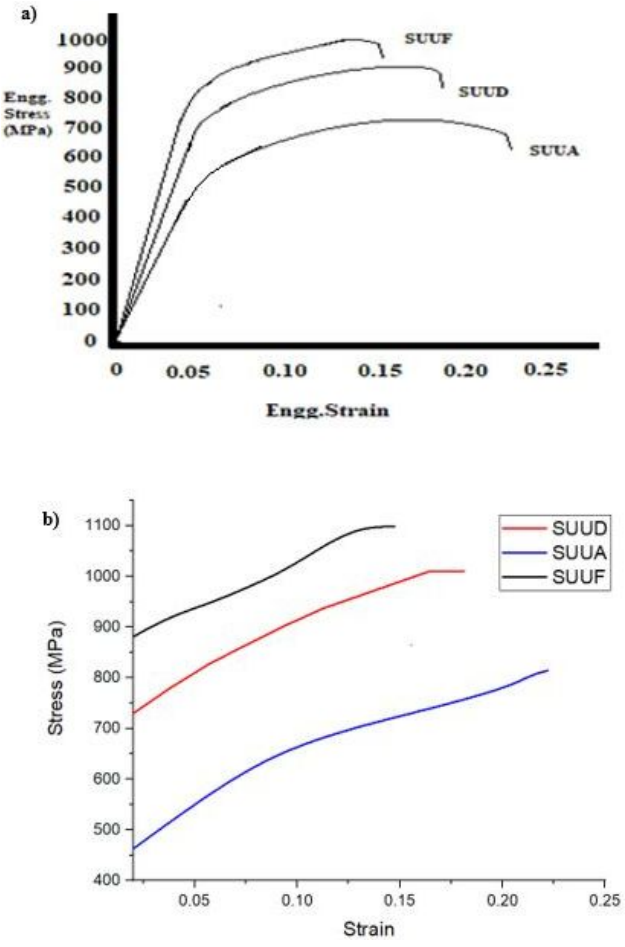

Figure 4: Stress-strain curves of welded joints; (a) Engineering stress-strain curve (b) Equivalent true plastic stress-strain curve.

Table 4: Transverse tensile properties of the welded joints

No.	Joint Type	0.2% Yield Strength (MPa)	Tensile Strength (MPa)	Elongation in 50 mm gauge length (%)	Flow Strength (MPa)	Notch Tensile Strength (MPa)	Notch Strength Ratio (NSR)	Failure Region
1.	SUUA	452	651	24	279	864	1.32	WM
2.	SUUF	886	962	16	631	1127	1.16	WM
3.	SUUD	712	856	20	447	1052	1.23	WM

joints showed superior ductility properties, and SUUF joints showed superior strength properties.

3.2 Impact toughness

The room temperature Charpy impact toughness of welded joints are presented in Table 5. Three specimens were tested in each condition, and the average of three results is presented. The SUUA joints showed the highest impact toughness of 72 J, which is 30 J higher than the base metal. SUUF joints showed the lowest impact toughness of 48 J. In conclusion, the SUUA joints exhibited superior impact toughness compared to SUUF and SUUD joints.

Table 5: Impact toughness properties of welded joints

Joint type	Charpy Impact Toughness (J) at Room Temperature
SUUA	72±4
SUUD	57±6
SUUF	48±4

Scanning electron microscopy (SEM) was used to analyse the mode of failure of tensile and impact toughness specimen as shown in Figure 5. The fractography shows all the specimen (Tensile and Impact) failed ductile mode with fibrous networks and fine equiaxed dimples, which indicates ductile mode of failure [22]. But the size of dimples varies in the joints. Fracture surface of SUUA joint shows a greater number of tiny dimples than other joints [23] and courser dimples with tear edges and shallow dimples with some flat facets [24] were observed in SUUF joint fractured surfaces.

3.3 Microhardness

The hardness measurement was carried out at four different regions, as shown in Figure 6 to identify variation in hardness across the joints. More than 10 readings were taken at close distances in each region. The lowest hardness was recorded in the weld metal region compared to HAZ, interface and BM regions. The SUUF joint recorded the highest hardness of 341 HV in the weld metal region. In contrast, the SUUA joint recorded the lowest of 236 HV.

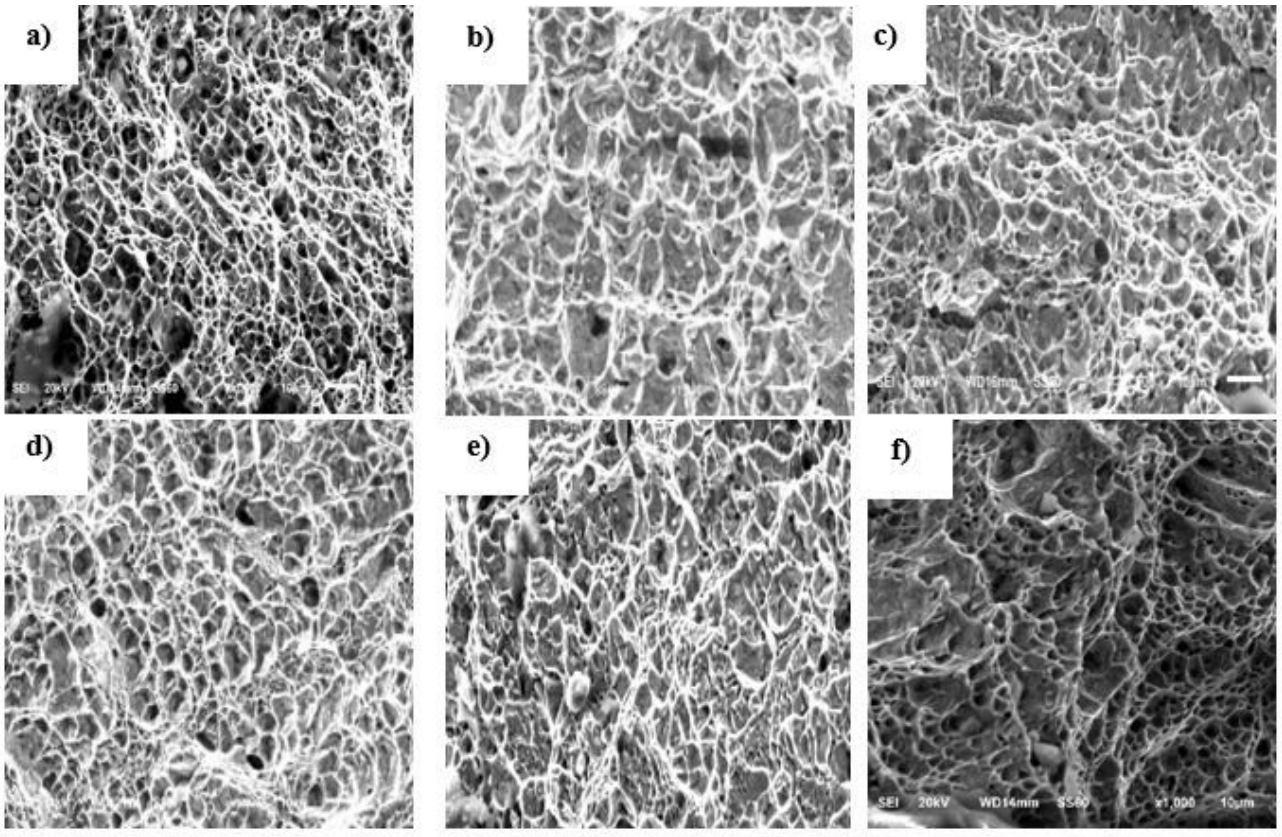

Figure 5: Fractographs of tensile and impact toughness tested specimens; (a) SUUA Joint-Tensile; (b) SUUD Joint-Tensile; (c) SUUF Joint-Tensile; (d) SUUA Joint-Impact; (e) SUUD Joint-Impact; (f) SUUF Joint-Impact

Table 6: Microhardness of various regions

	Weld Metal (WM)	Interface	CGHAZ	FGHAZ	ICHAZ	Base Metal (BM)
SUUA	236±3	652±8	756±6	812±4	808±7	601±2
SUUD	312±5	664±12	741±9	796±2	781±4	598±2
SUUF	341±4	512± 9	532±6	712±3	564±7	596±4

Lower hardness is the main reason for failure of tensile specimen at weld metal irrespective of the consumables. Hardness is much higher than base metal in fine grain heat affected zone (FGHAZ) in all the joints irrespective of the consumables. In coarse grain heat affected zone (CGHAZ), softening occurred appreciably in SUUF joint compared with SUUA and SUUD joint. In inter-critical heat affected zone (ICHAZ-(HAZ/BM interface)), the higher softening was observed in the SUUF joint compared with SUUA and SUUD joints. The reason for softening and hardening is mainly determined by heat input which controls the microstructural characteristics of the HAZ.

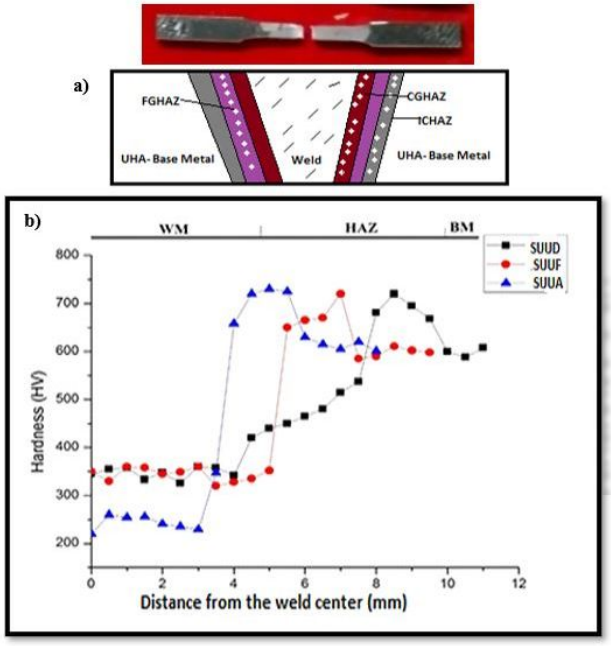

Figure 6: Microhardness survey; (a) Scheme of microhardness survey; (b) Hardness across weldment

3.4 Macrographs

Figure 7 shows the cross-sectional macrographs of welded joints. All the joints are free from macro-level defects such as lack of fusion, lack of penetration, porosity and cracks. The width of WM and HAZ were measured and presented in Table 7. Due to variation in the heat input, the width of the WM and HAZ of the joints are marginally varying. The joint fabricated using ASS consumable (SUUA) contains the lowest WM area compared to other two joints. SUUF joint

Table 7: Dimensions of weld metal and HAZ regions

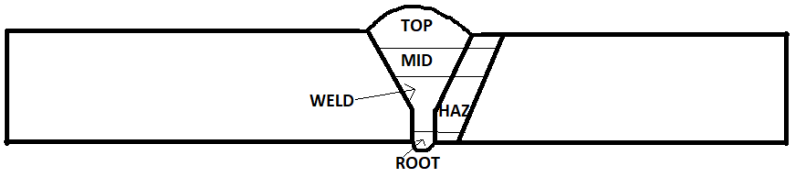

Joint	Weld Metal (WM) Zone				Heat Affected Zone (HAZ)			
	Width at top (mm)	Width at mid thickness (mm)	Width of root side (mm)	WMZ area (mm^2)	Width at top (mm)	Width at mid thickness (mm)	Width of root side (mm)	HAZ area (mm^2)
SUUA	20.5	7.2	2.9	142.3	1.2	2.5	3.5	51.2
SUUD	21	7.8	3.1	156.4	2.5	3.0	3.9	68.3
SUUF	24.13	11.6	4.6	205.8	2.8	5.8	5.6	89.1

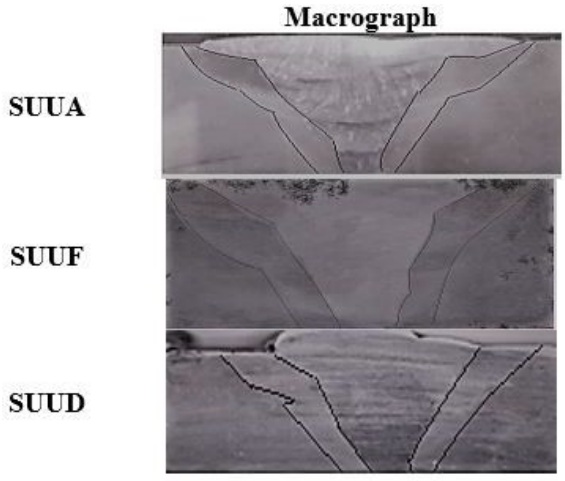

Figure 7: Macrostructure of weld joints

contains the highest WM area of (205.8 mm^2) among the three joints. The SUUA joint has the lowest HAZ area of 51.2 mm^2, and the SUUF joint has wider HAZ width area of 89.1 mm^2. It is necessary to obtain narrow HAZ and WM area to reduce soft zone width for better ballistic resistance.

3.5 Microstructure

From the microhardness survey, it is understood that weldment consists of five distinct regions (i) Weld Metal, (ii) CGHAZ (iii) FGHAZ (iv) ICHAZ, (v) BM.

(i) Weld Metal (WM)

Weld metal of SUUA and SUUD joint consists of the plain austenitic matrix and the secondary phase delta ferrite. The difference between SUUA and SUUD joint is the percentage of delta ferrite and its morphology. The weld region of SUUA joint is composed of vermicular delta ferrite, as shown in Figure 8a. The WM region of SUUD joint is composed of the mixture of lacy and vermicular delta ferrite (Figure 8c). There is a relationship between the volume percentage of delta ferrite and its morphology discussed in the upcoming section. The orientation of the residual phase depends on the heat flow direction, which enhances the primary dendritic growth, and these ferrites are located in the core of the primary dendritic arm [25]. The WM region of SUUF joint composed of the non-directional acicular ferrite in the austenitic matrix [26, 27], as shown in Figure 8e. Usually oriented (directional) and a large colony of lath structures are undesirable in weld metal which easily propagates the cracks [28–31].

The martensite in the weld metal is distorted. System energy is reduced to the maximum level, and phase separation occurs at interface with similar atomic spacing (results in unit cell axial ratio to unity-low carbon distort the martensite). These phases can't be a grain boundary phase; hence they separate within the grain boundaries. Moreover, ferrites are intergranular nucleating ferrite with a non-directional orientation, which gives acicular ferrite a small grain size, with non-directional lath. However, the acicular ferrite is the most preferred microstructure in the weld metal.

(ii) Interface

Figures 8b and 8d show the interface (WM-HAZ) of the SUUA and SUUD joints respectively. In both joints, towards HAZ, the untempered martensite with a martensitic band (MB) and white phase (unmixed zone (UMZ)) in the fusion line is observed. SUUF joints fabricated using low hydrogen ferrite (LHF) show sufficient dilution and more refined mixing at the interface due to similar crystal structures.

(iii) Heat Affected Zone (HAZ)

HAZ is divided into three regions (i) CGHAZ, (ii) FGHAZ, and (iii) ICHAZ. During the weld thermal cycle (heating and cooling), the CGHAZ region are heated to high temperature. At high-temperature region, coarser austenite grains retransform into coarser martensite in SUUA and SUUD (Figure 9a) joints and coarser martensite and bainite grains in SUUF joints. In FGHAZ, all the joints show martensite as the predominant phase with smaller grain size. As expected, the temperature exposed is much less at FGHAZ than the CGHAZ, which leads to the formation of martensite due to fast cooling (Figures 9b and 9d). The soft zone is formed at the interface of FGHAZ and BM (Figures 9e and 9f). At ICHAZ, where the hardness drops due to the formation of soft patches of white ferrite phase along with coarse martensite with reduced dislocation density due to exposure between (AC_1–AC_3) temperature during heating and cooling (thermal cycle) [32, 33]. At a particular temperatures dual-phase ($\alpha + \gamma$) and the recrystallization mechanism helps to transform tempered martensite to polygonal ferrite and martensite towards the base metal. The unaffected base metal consists of tempered martensitic lath structure.

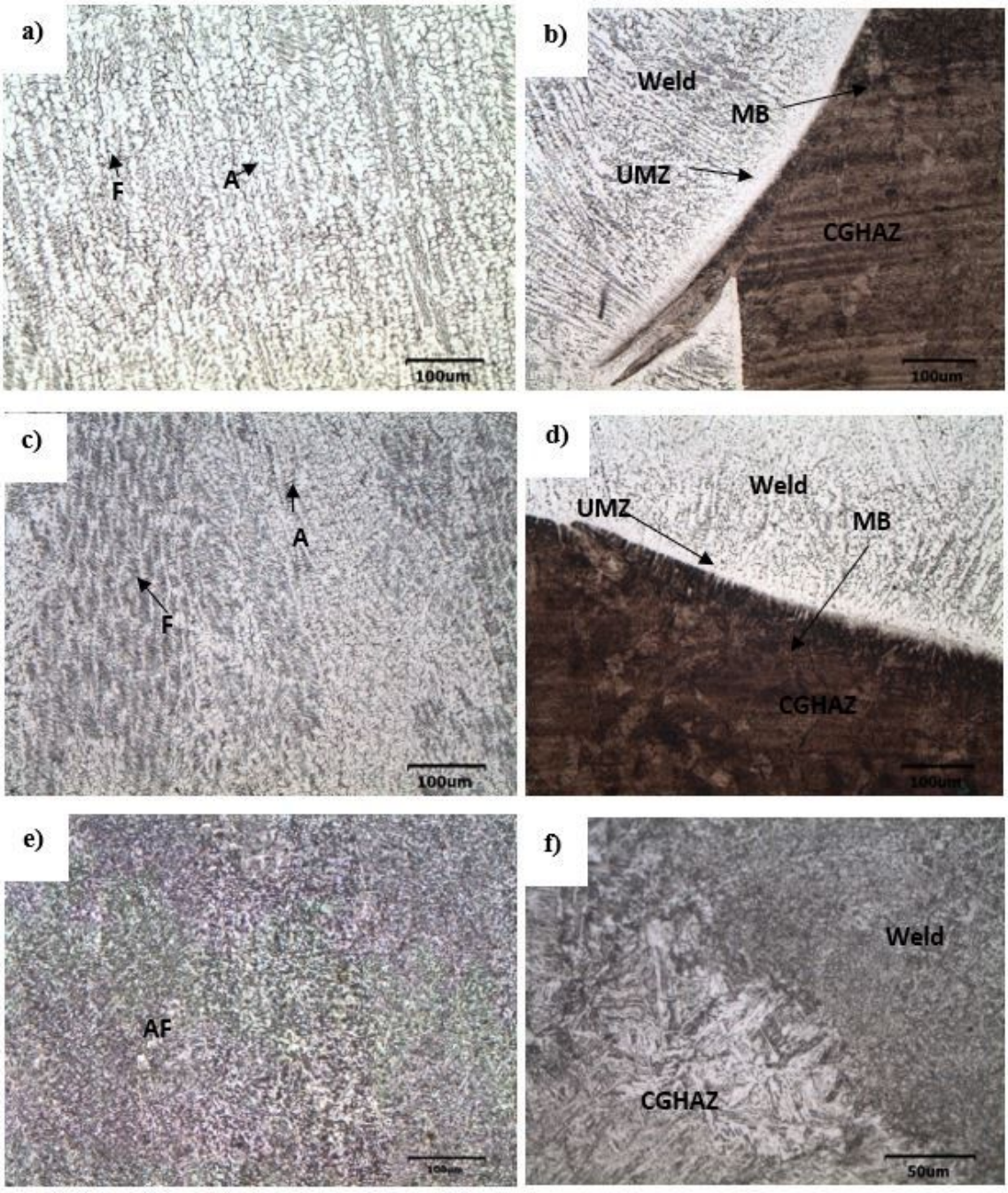

Figure 8: Optical micrographs of weld metal and interface of joints; (a) Weld metal of SUUA joint; (b) interface of SUUA joint; (c) Weld metal of SUUD joint; (d) interface of SUUD joint; (e) Weld metal of SUUF joint; (f) interface of SUUF joint

Table 8: Chemical composition (wt%) of weld metal measured by OES

Joint	Cr	Mo	Mn	Ni	Si	C
SUUA	20.12	2.12	2.31	8.29	0.49	0.081
SUUD	24.50	3.61	0.97	7.30	0.52	0.036
SUUF	0.101	0.245	1.50	2.01	0.212	0.051

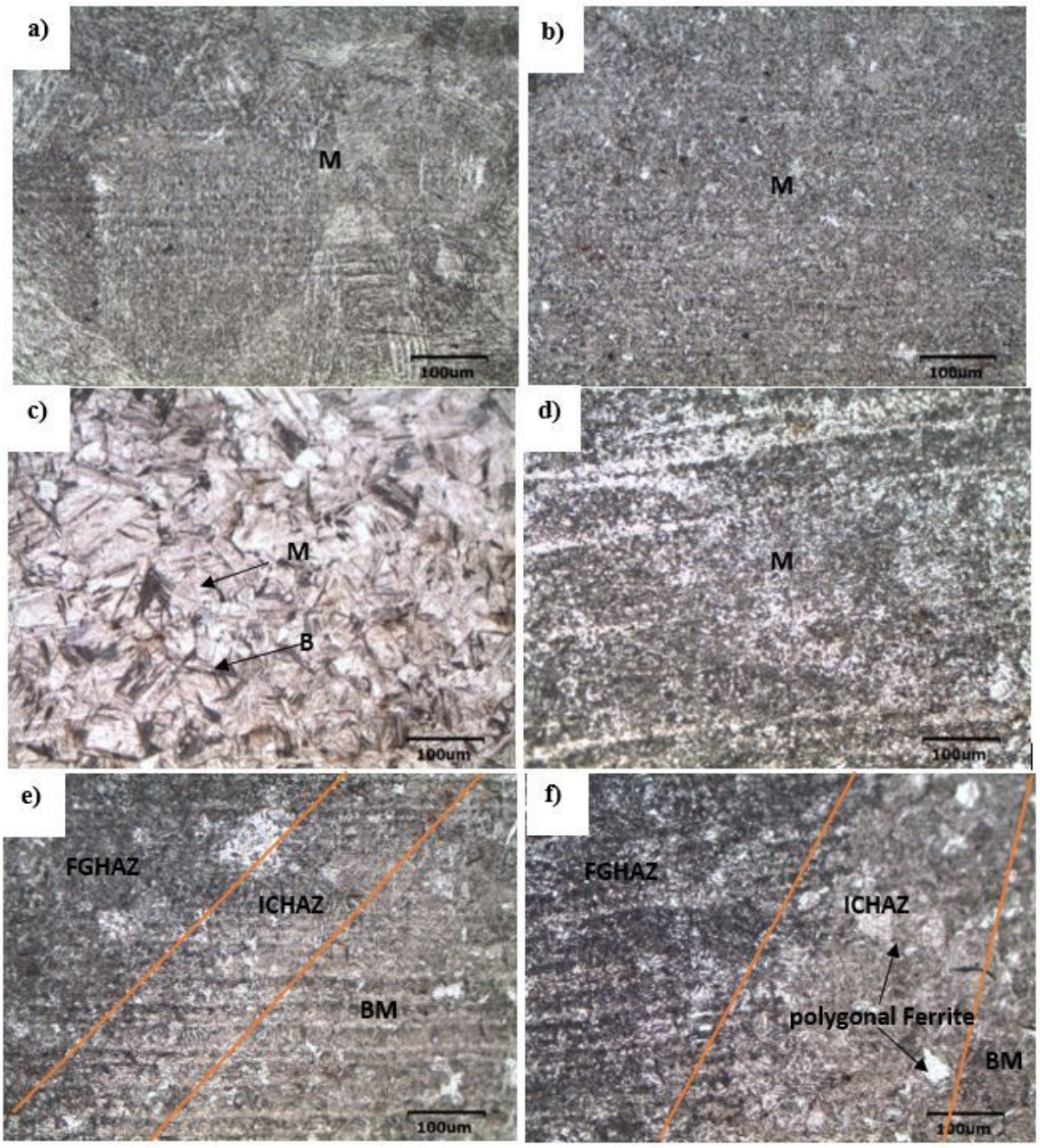

Figure 9: Optical micrographs of welded joint HAZ; (a) CGHAZ of SUUA joint; (b) FGHAZ of SUUA joint; (c) CGHAZ of SUUD joint; (d) FGHAZ of SUUD joint; (e) ICHAZ of SUUA joint; (f) ICHAZ of SUUD joint

Table 9: Cr_{eq}/Ni_{eq} ratio

Joint	Cr_{eq}	Ni_{eq}	Cr_{eq}/Ni_{eq}
SUUA (Schaeffler diagram)	22.97	12.27	1.87
SUUD (Schaeffler diagram)	28.88	8.86	3.2
SUUA (WRC-92)	22.24	11.12	2
SUUD (WRC-92)	28.11	8.56	3.28

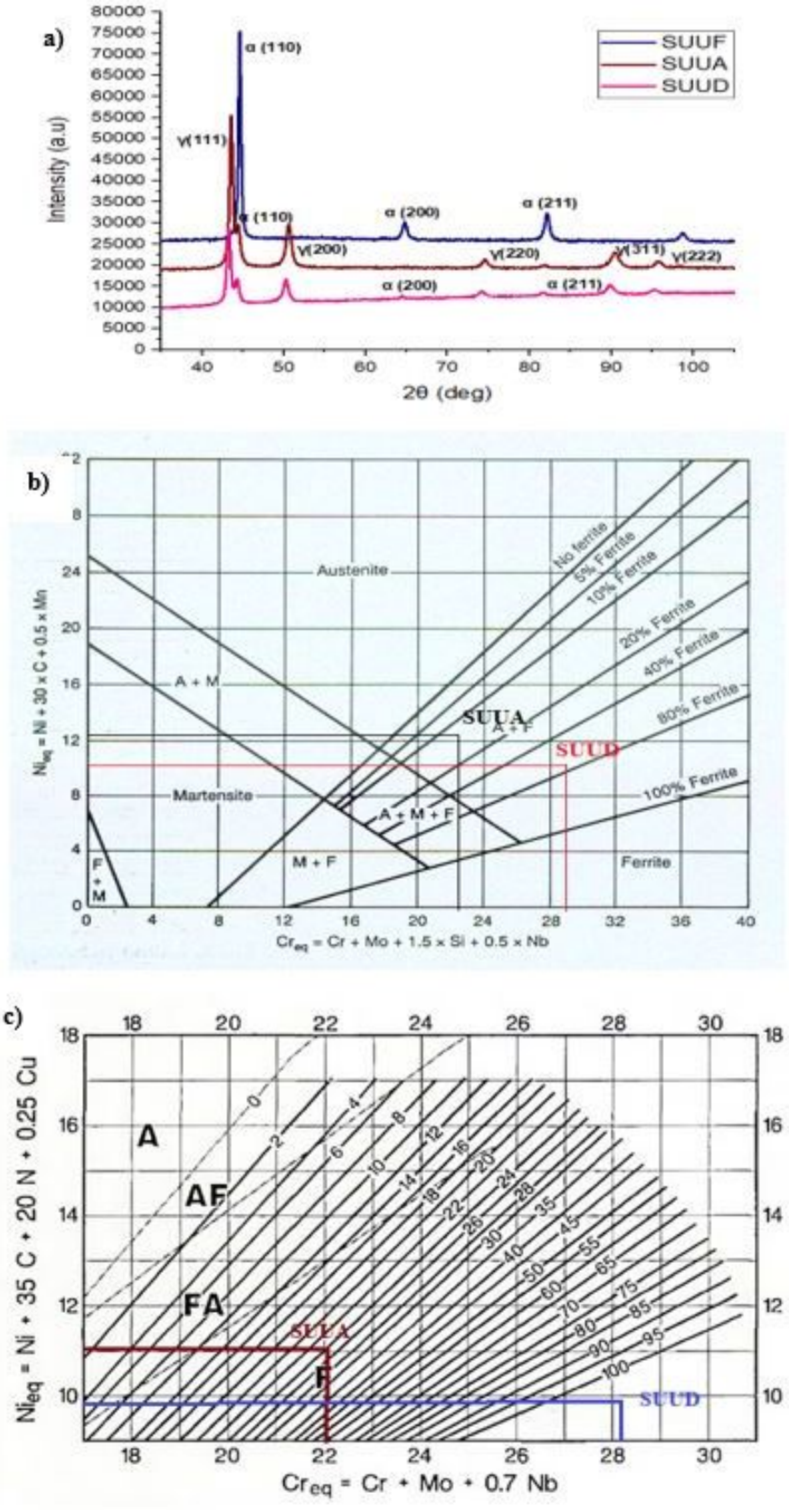

Figure 10: Weld Metal analysis; (a) XRD of joints; (b) Schaeffler diagram; (c) WRC-92 diagram

3.6 Chemical composition

The main difference between the SUUA and SUUD joint is the volume fraction of delta ferrite in the weld metal. It is vital to understand the chemical composition of weld metal after dilution (a small portion of base metal and a large portion of electrode). The dilution is depending on parameters heat input, base metal, welding consumables, type of welding joint (groove, fillet or weld overlay), joint edge preparation (square or V groove) and bevel angle. An optical emission spectrometer (OES) was used to analyze the weld metal chemical composition and the average values are presented in Table 8. The chemical composition was used to calculate the Cr_{eq}/Ni_{eq} ratio using the Eqs. (1) and (2) and presented in Table 9. Based upon the Cr_{eq}/Ni_{eq} ratio, the mode of solidification changes can be derived (directly affecting the mechanical properties of joints). X-ray diffraction (XRD) analysis (Figure 10a) shows austenite and ferrite in the weld metal of SUUD and SUUA joint. Whereas the SUUF joint mainly consists of ferrite phase. Schaeffler diagram (Figure 10b) and Welding Research Council-1992 (WRC-92) diagram (Figure 10c) was used to calculate the volume percentage of delta ferrite present in the weld metal of SUUA and SUUD joints. Calculated Ni_{eq} and Cr_{eq} in both diagrams are nearly same.

$$Ni_{eq} = Ni + (30 \times C) + (0.5 \times Mn) \quad (1)$$

(Schaeffler diagram)

$$Cr_{eq} = Cr + Mo + (1.5 \times Si) + (0.5 \times Nb) \quad (2)$$

(Schaeffler diagram)

$$Ni_{eq} = Ni + (35 \times C) + 20N + (0.25 \times Cu) \quad (3)$$

(WRC-92)

$$Cr_{eq} = Cr + Mo + (0.7 \times Nb) \quad (4)$$

(WRC-92)

$$L \rightarrow L + \delta \rightarrow \delta + \gamma \rightarrow \gamma \quad 1.48 - 1.95 \quad (5)$$

(FA mode)

$$L \rightarrow L + \delta \rightarrow \delta + \gamma \rightarrow \gamma \quad < 1.95 \quad (6)$$

(F mode)

4 Discussion

The joints fabricated using austenitic stainless steel (ASS) and super duplex stainless steel primary consist of plan austenitic matrix with residual delta ferrite irrespective of the process.

Nevertheless, grain size, morphology, solidification mode differs. When comparing SUUA and SUUD joints, secondary residual phases, delta ferrite percentage is higher in the SUUD joint. A high percentage of nickel and manganese can eliminate the formation of delta ferrite, and direct solidification of austenite is possible. The solidification completely changes from FA mode to F mode in SUUD with a Cr_{eq}/Ni_{eq} ratio of 3.2. This difference in the ratio alters the mechanical properties between these two joints. The core of dendrite is delta ferrite which formed at high temperature during solidification begins which are rich in chromium. As solidification proceeds further, the chromium content reduces. The delta ferrite present at room temperature reduces toughness and ductility due to the minimum solubility of a carbon atom at its atomic lattice. Hence the presence of austenite in the WM is essential to improve ductility and toughness. The austenitic phase is characterized by low hardness and low strength, whereas, ferrite is characterized by high strength and low ductility. HIC is a significant issue faced during the welding of armour steels. ASS consumables are useful to a great extent to dissolve the higher amount of hydrogen in its austenitic phase.

In joints fabricated using low hydrogen ferrite, weld metal predominately consists of acicular ferrite in the austenitic matrix in a non-directional way. It is known for interweaving ferrite plates, which cover a large proportion of the austenite matrix and imparts high strength and high toughness. Heat input controls acicular ferrite; as the heat input increases, the acicular ferrite decreases. Ferrite in the acicular form is mostly high angel boundaries, which deflect cracks due to non-directionally placed ferrite. Whereas the SUUF joint shows a finer acicular structure, which improves hardness and strength. The acicular structure was the main reason for obtaining high hardness along with strength in the weld metal of the SUUF joint. Dilution of weld metal to HAZ is an essential factor that determines the mechanical properties, cooling rate, and M_s temperature of the HAZ. Hence it is necessary to find the distribution of elements that alter the mechanical properties. Usually, in armour steels, each element has a different effect on the mechanical of the joint.

At interface, manganese improves hardenability and weak carbide former. Ni improves reliable solution strengthen, grain refiner, and strongly decreases the Ac_1 temperature. Along with carbon and molybdenum, chromium also has strong influences on hardenability [34]. In the SUUA joint at the interface, the centre of the fusion line is enriched with Cr, C, Mn, and Mo. Dilution was more significant (Cr, Mn, and Mo) in the interface. The migra-

tion in the elements towards the UHA interface favours the excessive formation of the martensitic band at the fusion line in the SUUA joint (interface) and increases hardness (Section 3.4). At the same time, Cr delays the softening from Fe_3C hardenability.

Chromium stabilizes the ferrite phase and delays the transformation temperature. The delta ferrite at the core of the dendrites, which form at the beginning of solidification, is very rich in chromium. However, the chromium content decreases as the solidification proceeds. The high amount of delta ferrite in welds reduces the toughness and drastically increases strength [35]. 3-20% of delta ferrite is essential in controlling the solidification cracking in the weld. Ni has a vital role in determining toughness. Nickel reduces the percentage of delta ferrite and stabilizes austenite in the SUUA joint. Future analysis exhibits a significant addition of manganese to determine the nickel advantage over stabilizing austenite. Another outcome of manganese as an alloying element increases the strength of the austenitic phase by substantial solution strengthening. These alloying elements control the solidification processes.

5 Conclusions

Ultra-high hard armour (UHA) steel are welded using shielded metal arc welding (SMAW) processes using three different consumables. From this investigation, the following conclusions are made.

1. Of the three joints investigated, the SUUF joint (fabricated using low hydrogen ferritic) exhibited superior strength properties (962 MPa) to other joints. High strength is associated with the presence of non-directional orientation of acicular ferrite in the weld metal region.
2. The SUUA joint (fabricated using austenitic stainless-steel electrode) exhibited more excellent ductility (higher percentage of elongation and NSR) and higher impact toughness (72 J) than other joints. This may be associated with the presence of high percentage of austenitic phase and vermicular delta ferrite in the weld metal region.
3. The tensile strength, notch tensile strength (NTS), and weld metal hardness of welded UHA steel joints revealed a directly proportional relationship with the Cr_{eq}/Ni_{eq} ratio of diluted weld metal. The ductility (elongation) showed an inversely proportional relationship with the Cr_{eq}/Ni_{eq} ratio.

Acknowledgement: The authors wish to record sincere thanks to the Directorate of Extramural Research & Intellectual Property Rights (ERIPR), Defence Research & Development Organisation (DRDO), Ministry of Defence, Government of India, New Delhi and Research Innovation Centre (RIC), DRDO, Chennai for the financial support rendered through a R&D project no: EPIR/EP/RIC/2016/1/M/01/1630. The authors are grateful to the Director, Combat Vehicles Research & Development Establishment (CVRDE), DRDO, Avadi, Chennai, for providing base materials to carry out this investigation.

Funding information: R&D project no: EPIR/EP/RIC/2016/1/M/01/1630.

Author contributions: All authors have accepted responsibility for the entire content of this manuscript and approved its submission.

Conflict of interest: The authors state no conflict of interest.

References

[1] Paul K, Markku P, Ramio S, Jukka M. Welding of Ultra High Strength Steels. Adv Mater Res. 2014;357-365.
[2] Magudeeswaran G, Balasubramanian V, Madhusudhan Reddy G. Effect of welding processes and consumables on fatigue crack growth behaviour of armour grade quenched and tempered steel joints. Def Technol. 2014;10:47-59.
[3] Fei Z, Pan Z, Cuiuri D, Li H, Wu B, Ding D, Su L, Gazder A.A. Investigation into the viability of K-TIG for joining armour grade quenched and tempered steel. J Manuf Process. 2018;32:482-493.
[4] Deb P, Challenger KD, Clark DR, Transmission Electron Microscopy Characterizations of Preheated and Non-Preheated Shielded Metal Arc Weldments of HY-80 Steel. Mater Sci Eng A. 1988;77:155-167.
[5] Madhusudhan Reddy G, Mohandas T, Tagore GRN. Weldability Studies on High-Strength Low-Alloy Steel Using Austenitic Stainless-Steel Filler. J Mater Proc Technol. 1995;1 49:213-228.
[6] Madhusudhan Reddy G, Mohandas T, Sarma D.S. Cold cracking studies on low alloy steel weldments effect of filler metal composition. Sci Technol Weld Join. 2013;8:407-414.
[7] Rao EJ, Guhab Malakondaiaha B. Effect of welding process on fatigue crack growth behaviour of austenitic stainless steel welds in a low alloy (Q & T) steel. Theor Appl Fract Mechan. 1997;2(27):141-148.
[8] Magudeeswaran G, Balasubramanian V, Balasubramanian T, Madhusudhan Reddy G. Effect of welding consumables on tensile and impact properties of shielded metal arc welded high strength, quenched and tempered steel joints. Sci Technol Weld Join. 2008;2(13):97-105.

[9] Tomków J, Fydrych D, Wilk K. Effect of Electrode Waterproof Coating on Quality of Underwater Wet Welded Joints. Materials. 2020;13(13):29-47.
[10] Tomków J, Fydrych D, Rogalski G, Labanowski J. Effect of the welding environment and storage time of electrodes on the diffusible hydrogen content in deposited metal. Revista de Metalurgia. 2019;55(1):140.
[11] U. Yadav, C. Pandey, N. Saini, J. G. Thakre, M. M. Mahapatra. Study on Hydrogen-Assisted Cracking in High-Strength Steels by Using the Granjon Implant Test. Metallogr Microstruct Anal. 2017;6:247–257.
[12] Magudeeswaranan G, Balasubramanian V, Sathyanarayanan S, Madhusudhan Reddy G, Moitra A, Venugopal S, Sasikala G. Dynamic Fracture Toughness of Armour Grade Quenched and Tempered Steel Joints Fabricated Using Low Hydrogen Ferritic Fillers. J Iron Steel Res. 2010;17:51-56.
[13] Magudeeswaran G, Balasubramanian V, Sathyanarayanan S, Madhusudhan Reddy G, Moitra A, Venugopal S, Sasikala G. Dynamic fracture toughness (JId) behavior of armour-grade Q&T steel weldments: Effect of weld metal composition and microstructure. Met Mater Int. 2009;15:1017–1026.
[14] Madhusudhan Reddy G, Mohandas T. Ballistic performance of high-strength low-alloy steel weldments. J Mater Process Tech. 1996;57:23-30.
[15] Verma J, Taiwade RV, Khatirkar RK, Kumar A. A Comparative Study on the Effect of Electrode on Microstructure and Mechanical Properties of Dissimilar Welds of 2205 Austeno-Ferritic and 316L Austenitic Stainless Steel. Mater Trans. 2016;57:494-500.
[16] Vashishtha H, Taiwade RV, Khatirkar RK, Dhoble AS. Effect of austenitic fillers on microstructural and mechanical properties of ultra-low nickel austenitic stainless steel. Sci Technol Weld Join. 2016;21:331-337.
[17] Inoue H, Koseki T, Ohkita S, Fuji M. Formation mechanism of vermicular and lacy ferrite in austenitic stainless-steel weld metals. Sci Technol Weld Join. 2000;5:385-396.
[18] Sathiya P, Kumar Mishra M, Soundararajan R, Shanmugarajan B. Shielding gas effect on weld characteristics in arc-augmented laser welding process of super austenitic stainless steel. Opt Laser Technol. 2013;45:46-55.
[19] Balakrishnan M, Balasubramanian V, Madhusudhan Reddy G. Microstructural Analysis of Ballistic Tests on Welded Armour Steel Joints. Metallogr Microstruct Anal. 2013;2:125–139.
[20] Balakrishnan M, Balasubramanian V, Madhusudhan Reddy G. Effect of hardfaced interlayer thickness on ballistic performance of armour steel welds. Mater Des. 2013;44:59-68.
[21] Razzak MA. Heat treatment and effects of Cr and Ni in low alloy steel. Bull Mater Sci. 2011;34:1439-1445.
[22] Lai CL, Lu WF, Huang JY. Effect of δ-ferrite content on the stress corrosion cracking behavior of cast austenitic stainless steel in high-temperature water environment. Corrosion. 2014;70:591–597.
[23] Das CR, Bhaduri AK, Srinivasan G, Shankar V, Mathew S. Selection of filler wire for and effect of auto tempering on the mechanical properties of the dissimilar metal joint between 403 and 304L(N) stainless steels. J Mater Process Technol. 2009;209(3):1428-1435.
[24] Karthick. K, Malarvizhi. S, Balasubramanian. V, Krishnan S.A, Sasikala. G and Shaju K. Albert et al. Tensile properties of shielded metal arc welded dissimilar joints of nuclear grade ferritic steel and austenitic stainless steel. J Mech Behav Mater. 2016;25(5–6):171–178.
[25] Balaguru V, Balasubramanian V, Sivakumar P et al. Effect of weld metal composition on impact toughness properties of shielded metal arc welded ultra-high hard armor steel joints. J Mech Behav Mater. 2020;29:186–194.
[26] Tushar S, Balasubramanian V, Malarvizhi S, Venkateswaran T, Sivakumar D, Effect of delta current and delta current frequency on tensile properties and microstructure of gas tungsten constricted arc (GTCA) welded Inconel 718 sheets. J Mech Behav Mater. 2019;28:186–200.
[27] Ramkumar KD, Oza S, Periwal S, Arivazhagan N, Sridhar R, Narayanan S. Characterization of weld strength and toughness in the multi-pass welding of Inconel 625 and Super-duplex stainless steel UNS S32750. Ciência & Tecnologia dos Materiais. 2015;27(1):41-52.
[28] Pujar MG, Dayal RK, Malhotra SN, Gill TPS. Dissolution behaviour of stainless steel weld metals during active potential range: a calculational approach. J Mater. 2000;35(3):735-746.
[29] Datta R, Mukerjee D, Mishra S. Weldability and toughness evaluation of pressure vessel quality steel using the shielded metal arc welding (SMAW) process. J Mater Eng Perform. 1998;7(6):817-23.
[30] Alipooramirabad H, Paradowska A, Ghomashchi R, Reid M. Investigating the effects of welding process on residual stresses, microstructure and mechanical properties in HSLA steel welds. J Manuf Process. 2017;(28):70-81.
[31] Viswanathan R, Henry JF, Tanzosh J, Stanko G, Shingledecker J, Vitalis B, et al. U.S. Program on materials technology for ultra-supercritical coal power plants. J Mater Eng Perform. 2005;(14):281–292.
[32] Laha K, Chandravathi KS, Parameswaran P, Rao KBS, Mannan SL. Characterization of microstructures across the heat-affected zone of the modified 9Cr-1Mo weld joint to understand its role in promoting type IV cracking. Metall Mater Trans A. 2007;(38):58–68.
[33] Shirmohammadi D, Movahedi M, Pouranvari M. Resistance spot welding of martensitic stainless steel:effect of initial base metal microstructure on weld microstructure and mechanical performance. Mater Sci Eng A. 2017;(703):154-61.
[34] Grajcar A, Morawiec M, Rozanski M, Stano S. Twin-spot laser welding of advanced high-strength multiphase microstructure steel. Opt Laser Technol. 2017;(92):52-61.
[35] Sarsilmaz F, Kirik I, Bati S. Microstructure and mechanical properties of armour 500/AISI2205 steel joint by friction welding. J Manuf Process. 2017;(28):131-6.